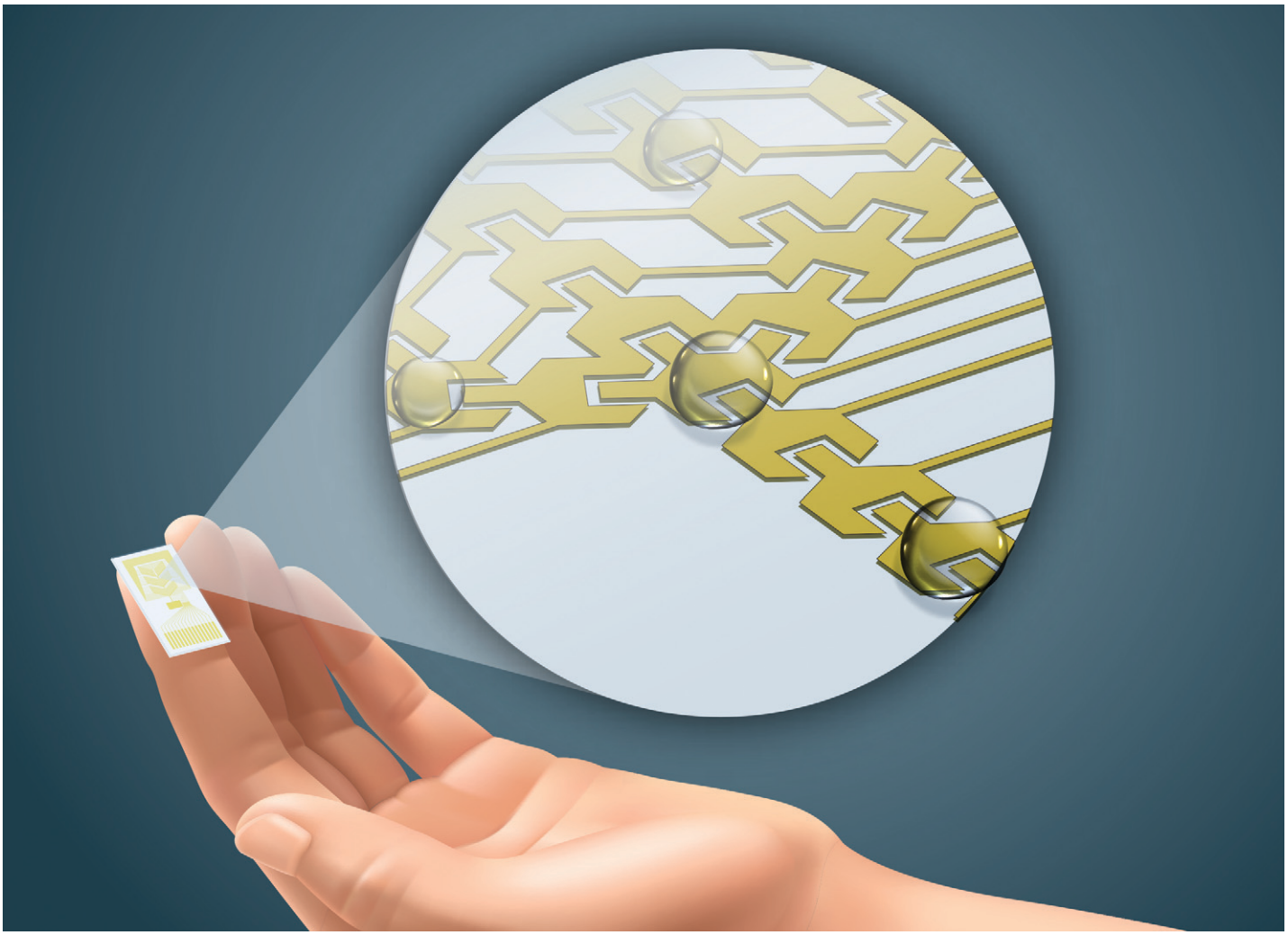

Showcasing research on wearable sweat sensing from Professor Jaap den Toonder's laboratory, Microsystems Research Section, Eindhoven University of Technology, the Netherlands.

Discretised microfluidics for noninvasive health monitoring using sweat sensing

Using sweat instead of blood for monitoring chemical biomarker concentrations of hospitalised patients offers great advantages for both patients and healthcare workers. However, these patients have extremely low sweat rates, which makes sweat sensing highly challenging. We propose a unique solution, by transporting the sweat in a discretised manner using electrowetting-on-dielectrics (EWOD). This method creates and moves 1 nanolitre sweat droplets from sweat glands to sensors integrated in the device while measuring sweat rate, under conditions typical for individuals at rest. *Artwork design by Inês Pereira.* Copyright holders: Inês Pereira and Jaap M.J. den Toonder.

As featured in:

See Jaap M. J. den Toonder *et al.*, *Lab Chip*, 2024, **24**, 5304.

ROYAL SOCIETY OF CHEMISTRY

rsc.li/loc

Registered charity number: 207890

Lab on a Chip

PAPER

View Article Online
View Journal | View Issue

Cite this: *Lab Chip*, 2024, **24**, 5304

Discretised microfluidics for noninvasive health monitoring using sweat sensing†

Emma J. M. Moonen, [ab] Walther Verberne,[c] Eduard Pelssers, [ac] Jason Heikenfeld[d] and Jaap M. J. den Toonder *[ab]

Received 13th September 2024,
Accepted 5th November 2024

DOI: 10.1039/d4lc00763h

rsc.li/loc

Using sweat instead of blood for monitoring chemical biomarker concentrations of hospitalised patients offers several advantages for both the patients and healthcare workers. Unlike blood, sweat can be noninvasively and continuously sampled without direct involvement of a professional, and sweat contains a rich composition of biomarkers. However, patients in resting state have extremely low sweat rates and they produce correspondingly small sweat volumes, which makes sweat sensing of hospitalised patients highly challenging. We propose a unique solution that enables the use of sweat as a viable biofluid for noninvasive health monitoring, by actively transporting the sweat in a discretised manner. Our device uses electrowetting-on-dielectrics (EWOD) to create and move sweat droplets with a volume of around 1 nanolitre from a sweat gland to sensors integrated in the device. We present the first wearable device with integrated EWOD, and we show that it can collect and transport sweat on-body, while measuring sweat rate, under conditions typical for individuals at rest.

1 Introduction

In modern healthcare facilities, monitoring the well-being of patients is of great importance and can be achieved by continuously measuring vital signs such as heart rate, oxygen saturation and blood pressure. These vital signs are measured by physical methods using electrodes and optical sensors integrated in (semi-)wearable devices, and the obtained data are immediately recorded on bedside monitors. However, monitoring the health status of patients often additionally requires periodic analysis of chemical biomarkers, mostly carried out by processing blood samples in the clinical laboratory of the hospital. The delay in receiving laboratory results can pose a significant challenge, especially when a patient's condition deteriorates rapidly. Furthermore, the drawing of blood does not always fit the workflow of the healthcare professional. Addressing these challenges and reducing the time gap between biofluid sampling and result acquisition calls for a novel approach: semicontinuous monitoring of chemical biomarkers that is noninvasive and imposes minimal workload on healthcare professionals. This approach must seamlessly integrate into hospital settings, ensuring timely and effective patient care.

Sweat emerges as a promising biofluid for addressing this need due to its rich composition of biomarkers and its noninvasive accessibility, making it an ideal candidate for semicontinuous health monitoring.[1–3] Despite its advantages, sweat sensing is not yet an established method for health monitoring in the clinic. The primary obstacle in developing wearable sweat sensing devices for monitoring hospitalised patients is the low sweat rate of people at rest, which is 0.1–3 nL min^{-1} per gland. Even if there are areas with a relatively high sweat gland density of approximately 100–500 glands per cm^2, such as the ventral forearm or the fingertips, only about 10% of these glands actively produce sweat in individuals at rest, resulting in a sweat rate of 1–150 nL min^{-1} cm^{-2}.[4–6] Hence, it is very challenging to realise a sweat sensing device for monitoring of hospitalised patients, since, depending on the specific use case there are certain requirements. This application requires a maximum delay time between the sample collection at the skin and the actual measurement of 15 to 30 minutes, and the generation of a measured data point every 5 to 30 minutes for a duration of the hospital stay ranging from several hours up to several days; additionally, existing integrated sensors typically require a sample of volume of at least 100 nL per measurement.

Most state-of-the-art continuous microfluidic sweat sensing devices are used to collect sweat in conditions with

[a] *Microsystems, Department of Mechanical Engineering, Eindhoven University of Technology, 5600 MB Eindhoven, The Netherlands. E-mail: j.m.j.d.toonder@tue.nl*
[b] *Institute for Complex Molecular Systems (ICMS), Eindhoven University of Technology, 5600 MB Eindhoven, The Netherlands*
[c] *Philips Research, Royal Philips, High Tech Campus, 5656 AE Eindhoven, The Netherlands*
[d] *Novel Devices Laboratory, Biomedical Engineering Dept., Univ. of Cincinnati, Cincinnati, Ohio 45221, USA*

† Electronic supplementary information (ESI) available. See DOI: https://doi.org/10.1039/d4lc00763h

high sweat rates, typically 1 μL min^{-1} cm^{-2}, such as during exercise or through iontophoretic stimulation. When these devices are used on individuals in resting state, it would take a couple of days to accumulate a sweat volume of 100 nL at the biosensor location for analysis. Consequently, obtaining clinically relevant information in a timely manner remains nearly impossible with devices based on continuous microfluidics. A few attempts have been reported in the literature to address sweat sensing in the medium to low sweat rate regime.[7–13] These approaches all use capillary driven flow to achieve passive collection and transport of the sweat. Examples are paper-based microfluidic devices,[7] the use of patterned fabrics integrated in a wearable microfluidic device,[8] including microfluidic capillary pumping structures in the device, such as micropillars or microchannels,[9–11] and, recently, the integration of a hybrid Janus membrane in a wearable sweat sensing device to pull sweat into the device.[12] Another device targeting sweat collection at low sweat rates, proposed by Peng *et al.*,[13] uses a layer of oil on the skin to fill the dead volume and to avoid sweat leaking between the skin and the device. In these devices, the required sweat volumes are still relatively large and/or the delay time is long, not fulfilling the requirements mentioned above. Some approaches, *e.g.*, Peng *et al.*,[13] still require iontophoretic stimulation of sweat production. Indeed, sweat production can be stimulated with pilocarpine or carbachol iontophoresis, which enables the use of sweat sensing devices for individuals at rest, and without the need for exercise to stimulate sweating.[14] However, iontophoretic stimulation does not deliver a stable flow rate for more than several hours which is often too short for patient monitoring[15] and the sweat rate in itself can not be used as health indication if sweating is stimulated as it is artificially increased. Importantly, all of the previous wearable sweat sensing devices rely on passive handling of sweat, which limits control over the process.

We present a novel approach based on active handling of sweat using discretised microfluidics, designed to facilitate the use of sweat for semicontinuous and noninvasive health monitoring with minimal sweat volumes, which fulfils the requirements mentioned above (Fig. 1A–C). Our method involves discretised sampling of sweat from individual glands and collecting it in inlet holes each having a volume of 8.2 nanolitres. Subsequently, we employ electrowetting-on-

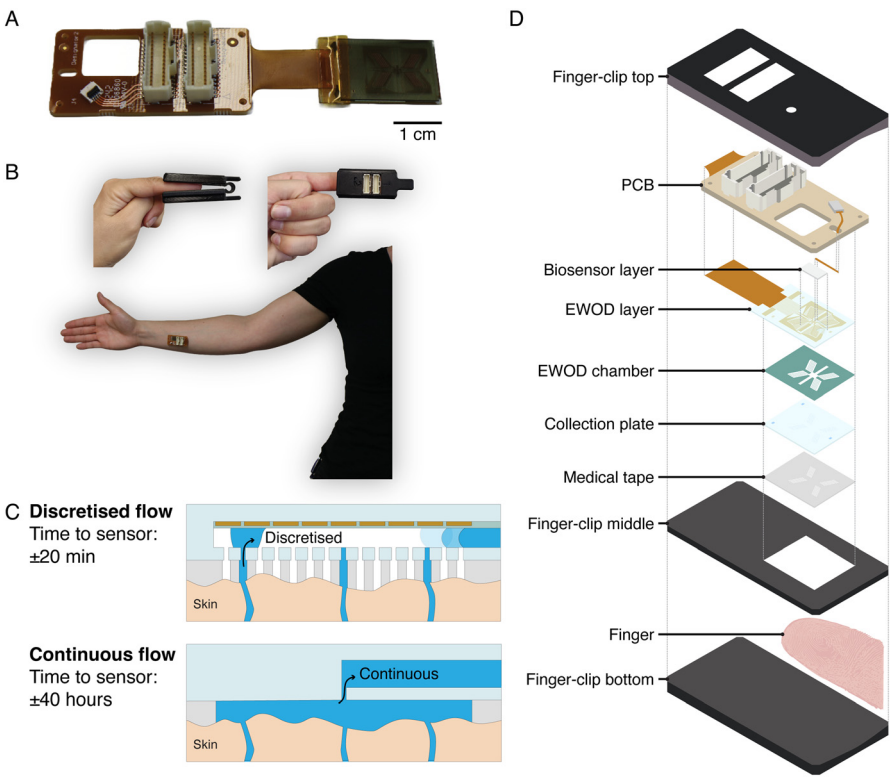

Fig. 1 Wearable sweat sensing device based on discretised microfluidics for noninvasive health monitoring. (A) Photograph of the integrated device. The medical tape and biosensor layer (shown in panel (D)) are not included for visibility. (B) The device can be attached to different body parts, such as the finger or the arm. (C) If a conventional microfluidic chamber with a height of 50 μm is placed on the skin with a surface area of 1 cm^2, to sample 10 glands excreting at a sweat rate of 0.2 nL min^{-1} per gland, it takes approximately 40 hours to fill, which is too long to deliver meaningful clinical information. We have designed a discretised solution, which utilises multiple small collection chambers on the skin with a volume that fills in 15–30 minutes, combined with fast transport of droplets using electrowetting-on-dielectrics (EWOD). This discretised solution enables the use of sweat sensing for clinical applications. (D) Schematic of the layer assembly of the wearable sweat sensing device. A printed circuit board (PCB) is attached to the glass electrodes using anisotropic conductive film (ACF) bonding to connect the actuation hardware *via* a cable. A 3D printed finger-clip is presented to clamp the device to the fingertip. Medical tape can also be used for fixation to different body parts.

dielectrics (EWOD) to create sweat droplets by pinching of sweat from the sweat that bulges out of a collection hole. Using EWOD, these droplets are then individually transported within seconds in the EWOD chamber, over a sweat rate sensor, and towards a biosensor chamber. The droplets accumulate in this biosensor chamber, in which a sensor can be integrated to measure chemical biomarker concentrations in a semicontinuous manner. The typical time between sweat production from a gland and arrival at the sensor is 20 minutes, two orders of magnitude smaller than for continuous microfluidics, see Fig. 1C. Being able to leverage small sweat volumes potentially also allows for lab-on-chip functionality, with advantages of integrating assays with reagents with excellent performance over simple electrochemical sensors. We show on-body proof of principle of an integrated wearable sweat sensing device which can collect, transport and detect droplets of sweat. The developed device enables usage of low volumes of sweat for analysis and provides a platform to use sweat for noninvasive health monitoring. The application of EWOD on this scale of hundreds of electrodes transporting droplets in the nanolitre range and in a wearable device is a unique combination which has never been presented before.

The device consists of several layers, schematically represented in Fig. 1D, each having a different function and design. The device is attached to the skin with a medical tape. Sweat enters the device *via* holes in this medical tape, and then through the collection holes of the collection plate that is made of glass. Each hole in the tape is aligned with one hole in the collection plate. On top of the collection plate, a chamber structure is made with double sided tape and dry film photoresist, called the EWOD chamber. The EWOD layer is placed on top of the EWOD chamber. The EWOD layer contains the electrodes and dielectric materials which are necessary for the transport of the droplets. The sweat exits the EWOD chamber *via* a hole to the biosensor layer which contains a chamber in which a biosensor and a waste absorber can be mounted. A printed circuit board (PCB) facilitates the connection of the glass EWOD layer to the control hardware. When the device is used on the finger, a 3D printed finger-clip is used to make sure that the device does not move.

2 Materials and methods

2.1 Materials and reagents

All chemicals and solvents were purchased from commercial suppliers and used as received, unless stated otherwise. Fused silica wafers and glass slides were purchased from Siegert wafer. 45% potassium hydroxide, AF1600, FC70 and silicone oil were purchased from Merck Life Science. MaN 440 photoresist, MaD 533-s developer, and hexamethyldisilazane (HMDS) were purchased from Microresist technologies. Acetone, isopropanol, Ordyl SY320 and Ordyl SY developer were purchased from MicroChemicals. Parylene dimer DPX-C was purchased from Speciality Coating Systems. Gold and chromium targets were purchased from IAM Drijfhout.

2.2 EWOD layer fabrication

A fused silica substrate with a thickness of 0.4 mm was machined using a femtosecond laser (FEMTOprint) and subsequently etched for 4 hours in 45% potassium hydroxide solution at 85 °C to create the outlet holes and the biosensor chamber. After oxygen plasma treatment and DI water rinsing, the substrates were treated with hexamethyldisilazane to improve wetting and adhesion of the photoresist. Next, photoresist MaN 440 was spincoated and baked for 2 minutes at 110 °C. The pattern in the photomask was aligned with the biosensor layer structures and exposed using a mask aligner (MJB4, SUSS MicroTec). The photoresist was developed in MaD 533-S developer for 2 minutes at room temperature. Au electrodes were defined by thermal evaporation (Nexdep, Angstrom Engineering) of Cr (5 nm) and Au (50 nm) and subsequent lift off of the photoresist in acetone. A 250 nm silicon nitride layer was deposited (16.5 sccm SiH_4, 13.5 sccm NH_3, 980 sccm N_2, 20 W, 650 mTorr, 300 °C) using plasma enhanced chemical vapour deposition (PE-CVD) (Plasmalab System 100, Oxford Instruments). A glass shielding mask was used to shield the connection pads during the PE-CVD process. Subsequently, a 500 nm thick parylene C layer was deposited by chemical vapour deposition (SCS Labcoter, Speciality Coating Systems). Surface protection tape (Micro to Nano) was used to shield the contact pads during the parylene deposition process. A double-layer dielectric stack of parylene C and SiN was used to yield EWOD actuation at low voltages, while maintaining electrowetting reliability by preventing electrical breakdown.[16] Finally, a thin layer (20–50 nm) of AF1600 1 wt% in FC70 was spincoated at 3000 rpm for 1 minute and annealed for 30 minutes in a vacuum oven at 130 °C. The selection of Teflon AF1600 as the hydrophobic layer was based on a preliminary study we performed of different options, namely AF1600, Cytop and Fluoropel 1601 V. The reason for the selection was the apparent improved overall performance with sweat for AF1600.[17]

2.3 Collection plate fabrication

A fused silica substrate with a thickness of 0.4 mm was machined using a femtosecond laser (FEMTOprint) and subsequently etched for 4 hours in 45% potassium hydroxide solution at 85 °C, to create the inlet holes. Next, a uniform layer of Cr (2 nm) and Au (10 nm) was deposited using a sputtercoater (Q300T D, Quorum Technologies). A layer of Ordyl SY320 dry film resist was then laminated (3600 pro, GBC) onto the substrate and the pattern in the photomask was aligned with the structures in the glass and exposed using a mask aligner (MJB4, SUSS MicroTec). After a 1 minute post-exposure bake at 85 °C, the dry film was developed in SY developer to define the spacer structures. Finally, a thin layer (20–50 nm) of AF1600 1 wt% in FC70 was

spincoated and annealed for 30 minutes on a hotplate at 130 °C.

2.4 Assembly of the sweat sensing device

A 25 μm thick spacer tape (ARcare 92734, Adhesives Research) was cut using a CO_2 lasercutter (VLS 3.50, Universal Laser Systems) to define the EWOD chamber. The tape was manually aligned on the EWOD layer and subsequently the collection plate and EWOD layer were aligned and bonded using a mask aligner (MJB4, SUSS MicroTec). The PCB was attached to the EWOD layer using ACF bonding. Conductive ink (Electric paint, bare conductive) was placed on the outer contact pads to make an electrical connection between the collection plate electrode and the outer connection pads of the EWOD layer. Conformal coating (Dow Corning 1-2577 Low Voc) was applied to the connection pads for insulation. By flushing the chamber with 20 cSt silicone oil, the surface of the EWOD chamber was impregnated. Glass plugs were machined with a femtosecond laser (FEMTOprint) and subsequently etched in 45% potassium hydroxide solution at 85 °C. The plugs were manually put in place into the outlet holes using tweezers under a microscope. Medical tape (1587, 3 M) was lasercut (VLS 3.50, Universal Laser Systems) and manually aligned to the collection plate under a microscope. A schematic drawing of all the layers of the device is displayed in Fig. S6.†

2.5 Electronic system and interface design

A dedicated setup was used for actuation of the wearable sweat sensing device and acquisition of the sensor signals. The electronic system, schematically depicted in Fig. S4,† contains three main parts: the control printed circuit board (PCB), the actuation and signal acquisition hardware, and two computers. Details are provided in the ESI.†

2.6 Artificial skin testing

The wearable sweat sensing devices were tested on an earlier developed artificial skin platform.[18] This artificial skin platform was controlled using a pressure based microfluidic flow controller (MFCS-EXZ, Fluigent). During testing on the artificial skin, DI water was used as a proxy for sweat, see section 3.2 for the rationale behind this choice.

2.7 On-body study

The evaluation of the wearable devices was performed using healthy human volunteers in accordance with the protocols and approval of the Ethical Review Board (ERB) at Eindhoven University of Technology (Ref:ERB2022ME2 and ERB2023ME4). Iontophoretic sweat stimulation was performed using the Macroduct Advanced system (Elitech group) according to approval from the Ethical Review Board (ERB) at Eindhoven University of Technology (Ref: ERB2022ME4). All subjects provided written informed consent before participation in the study. For all the human studies, the subjects cleaned their skin with water and soap and acetone swabs, and the investigator applied a thin layer of petroleum jelly (Vaseline) before applying the wearable device on the skin.

2.8 Sweat collection

Sweat was collected from healthy volunteers using ionthophoretic stimulation (Macroduct Advanced, Elitech group), for transport and sensor characterisation. The sweat collection was conducted according to approval from the Ethical Review Board (ERB) at Eindhoven University of Technology in accordance with the protocol (Ref: ERB2022ME4). All subjects provided written informed consent before participation in the study.

3 Results and discussions

3.1 Design of the skin-device interface

The initial step to be performed by a wearable sweat sensing device involves the collection of sweat. A significant challenge in this process is the efficient sweat collection from individuals at rest within a reasonable time frame. To put this into perspective, a microfluidic collection chamber placed on the skin with a surface area of 1 cm^2 and a height of 50 μm has a volume of 5 μL. While this volume may seem small, the sweat rate from individual sweat glands on the forearm of a resting person is only approximately 0.2 nL min^{-1} per gland and approximately 10 glands per square centimetre are actively producing sweat.[5] This implies that it would take approximately 40 hours to fill this microfluidic collection chamber, which is much more than the required maximum delay of 15 to 30 minutes mentioned in the introduction. Increasing the surface area of the collection chamber may be an approach to involve more glands, but this also increases the chamber volume and thus provides no net benefit towards reducing the filling time. Decreasing the surface area reduces the chamber volume, but also the number of sampled glands and it increases the chance that no sweat glands are sampled at all. Furthermore, sweat transport by sweat gland pressure *via* continuous flow in microchannels towards biosensors is slow, and diffusion processes will make time-resolved measurements difficult. Therefore, state-of-the-art sweat sensing devices based on continuous microfluidics, as reported in literature, can only work with athletes, otherwise heat-stressed individuals or by iontophoretic stimulation which results in sweat rates up to 50–100 times that of individuals at rest.

Our discretised sweat collection method is based on using multiple circular holes in a collection plate, each with a diameter similar to that of a sweat gland exit onto the skin, as opposed to a single large microfluidic chamber as is used in continuous microfluidics. This approach enables the sampling of sweat from a large skin area while maintaining a low filling volume, as the holes not connecting to a sweat gland will not fill. It is crucial to design the skin-sweat-device interface in such a way that the sweat successfully enters the

device while sweat loss through leakage over the skin is minimised. It is furthermore essential that the design is compatible with the EWOD transport, and that there are enough collection holes to collect sufficient sweat for sensing and to mitigate the possibility of not sampling any sweat glands.

To aid the design of the collection plate, we model the skin-sweat-device interface using a burst valve model, illustrated in Fig. 2A. The burst valves (triangles) represent the required Laplace pressures for the liquid front to pass a certain position. The resistances (rectangles) represent the hydrodynamic resistances of channels and chambers. For successful entry of sweat into the device and eliminating leakage, it is essential that the Laplace pressures on the liquid fronts entering the collection plate (ΔP_i) and entering the EWOD chamber (ΔP_c) are both smaller than the Laplace pressure on the liquid front between the skin and the device, or the leakage exit (ΔP_L), *i.e.*, ΔP_i & $\Delta P_c < \Delta P_L$. Furthermore, both the Laplace pressure for the sweat entering the inlet hole and that for entering the EWOD chamber must be smaller than the pressure delivered by the sweat gland P_g which drives the entire entry process, *i.e.*, ΔP_i & $\Delta P_c < P_g$.

A maximum pressure delivered by the sweat glands of up to 70 kPa is reported in the literature, determined during chemical stimulation and under no flow condition.[20,21] A more recent publication of an experimental study found average values of secretory fluidic pressures generated at the surface of the skin by eccrine sweat glands in healthy young adults between 2.4 and 2.9 kPa.[22] In our model we assume an average maximum pressure delivered by the sweat glands of P_g = 2.65 kPa.

The Laplace pressures in the burst pressure model can be expressed in terms of the dimensions of the device features, the contact angles of the sweat with the different surfaces of

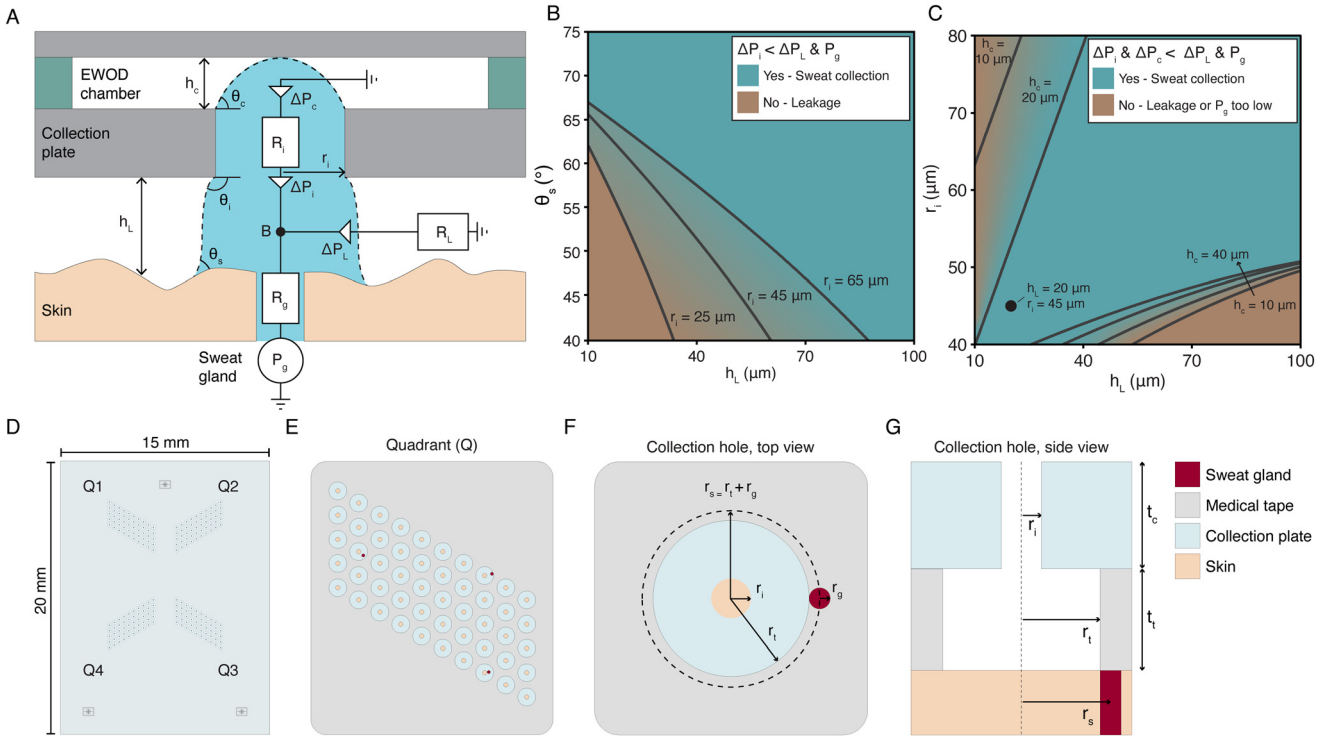

Fig. 2 Design of the skin-device interface. (A) Schematic illustration of the burst valve model to describe the entry of sweat into the device. ΔP_c, ΔP_i, and ΔP_L represent the Laplace pressures for entry into the EWOD chamber, entry into the inlet hole, and leakage over the skin, respectively. R_g, R_i, and R_L represent the hydrodynamic resistances of the sweat gland duct, the inlet hole in the collection plate, and the leakage exit over the skin. θ_s, θ_i, and θ_c represent the contact angles of the skin, the contact angle of the inlet hole and the bulging angle of the protrusion to reach the top of the EWOD chamber with a height h_c. h_L is the height between the collection plate and the skin, r_i is the radius of the inlet hole, and P_g is the pressure delivered by the sweat gland. The symbol B indicates the bifurcation from the sweat gland to either the inlet hole or the leakage exit over the skin. (B) Solution space for the sweat entering the inlet hole in the collection plate, $\Delta P_i < \Delta P_L$ & P_g, for non-hydrated skin contact angles θ_s between 40 and 75°. The lines represent the boundaries for which $\Delta P_i = \Delta P_L$ for different radii of the inlet (r_i). (C) Solution space for the sweat entering both the inlet hole and the EWOD chamber, ΔP_i & $\Delta P_c < \Delta P_L$ & P_g. The contact angle of the skin (θ_s) is fixed at 102°, representing skin treated with petroleum jelly, and $r_t = r_i$; r_t is defined in panels F and G. The lines represent the boundaries for which ΔP_i & $\Delta P_c < \Delta P_L$ & P_g does not hold anymore for different heights of the EWOD chamber (h_c). It is assumed that P_g = 2.65 kPa. The circular marker represents the dimensions of the final design. (D) Schematic drawing of the full collection plate. Each device has four quadrants (Q1–4). (E) Schematic drawing of one of the quadrants, containing 50 collection holes. (F and G) Schematic drawing of the top (F) and side (G) view of a single collection hole. The inlet hole in the glass collection plate has a radius r_i of 45 μm and the hole in the medical tape has a radius r_t of 150 μm. The thickness of the medical tape and the collection plate are t_t = 80 and t_c = 400 μm respectively. A sweat gland exit, with a typical radius r_g of 25 μm,[19] is schematically represented by a red circle.

the device, and the surface tension of the sweat. The corresponding equations and the details of the model can be found in the ESI.† Fig. 2B shows the solution space for entry into the inlet hole in the collection plate, $\Delta P_i < \Delta P_L$ & P_g, as calculated using the model for a varying height between the skin and the device h_L, contact angle of the skin θ_s, and radius of the inlet hole r_i. Skin is normally hydrophilic,[18] hence the range for θ_s is set between 40 and 75°. Clearly, Fig. 2B shows that when both the inlet hole radius and the skin-device gap are small, as is desired to reduce the initial filling volume, the sweat will not enter the device but will start leaking on the skin. We have solved this issue by applying petroleum jelly on the skin before attaching the device, since this increases the contact angle of the skin to θ_s = 102°, so that the condition for entry in the inlet hole is fulfilled even for small h_L and r_i, as can be seen from Fig. 2B. We experimentally verified the necessity of petroleum jelly on the skin, as is described in the ESI.† In addition, we have added a hydrophobic double sided medical tape with thickness t_t on the collection plate, with openings to the inlet holes, which conforms to the skin and maintains a small gap height. Considering these measures, Fig. 2C shows the solution space for entry both into the inlet hole and into the EWOD layer, ΔP_i & $\Delta P_c < \Delta P_L$ & P_g. Clearly, successful entry of sweat into the device is possible for a range of values of inlet hole radius r_i, skin-device gap h_L, and EWOD channel height h_c. The values are chosen to have small filling volumes for achieving short filling times.

The device presented here is designed for application on the fingertip, because there the sweat gland density and sweat rate are high compared to other body locations.[5] The tips of the finger have the highest eccrine sweat gland density on the body, with on average 530 glands per cm^2. Assuming that only 10% of the sweat glands will actively produce sweat in resting state, there are approximately 50 active glands per cm^2 on the fingertip of individuals in resting state.[4] For the sweat rate in resting state, Burch *et al.*[6] measured 150 nL min^{-1} cm^{-2} on the index fingertip; assuming 50–500 active glands, this corresponds to 3–0.3 nL min^{-1} per gland. Taylor *et al.*[5] report the sweat rate of the total palm of the hand; a sweat rate of 0.5 nL min^{-1} per gland was reported for resting, passively heated individuals, and a sweat rate of 2 nL min^{-1} per gland was reported during dynamic and static exercise. Taking together all the available data, we assumed a range of sweat rate per gland between 0.3 and 3 nL min^{-1} per gland, and 50 active glands cm^{-2} as typical values for the fingertip of individuals at rest to design the skin–device interface. These values correspond to a sweat rate per skin area of 15 to 150 nL min^{-1} cm^{-2}. Fig. 2D–G shows the final design of the collection plate and the medical tape. The initial volume that must be filled by a gland before the sweat enters the EWOD channel, equals the sum of the volumes of the hole in the medical tape and that of the inlet hole in the collection plate, *i.e.*, $t_t\pi r_t^2 + t_c\pi r_i^2$, where t_t and t_c are the thickness of the tape and of the collection plate, respectively. The filling volume must be small to minimise the delay time between sampling and first sensor readout. Fig. 2C shows that the minimum radius of the holes in the collection plate (r_i) should be approximately 45 μm for the sweat to enter successfully in the device. The radius of the holes in the medical tape is set at r_t = 150 μm; this choice is based on the fabrication possibilities, and the geometry of the EWOD layer. The thickness of the medical tape and the collection plate are t_t = 80 μm and t_c = 400 μm respectively, which results in total volume of 8.2 nL per collection hole assuming an average space between the skin and the collection plate of the thickness of the tape. Hence, for a sweat rate of 0.3 and 3 nL min^{-1} per gland, the initial filling time ranges between 27 and 2.7 minutes, assuming that there is one gland present in the hole. This is within the acceptable range of the required maximum delay time up to 30 minutes, mentioned in the introduction. The final design (r_i = 45 μm, t_t = 80 μm, and h_c = 25 μm, see the next section) is indicated in Fig. 2C with a circle. The final design aspects concerns the number of collection holes, which determines the average number of sampled glands and therefore the total sweat volume collected. With 200 collection holes, the average number of sampled glands is between 2 and 20, depending on the expected active glands per cm^2 (see the ESI† and Fig. S2). For 50 active glands per cm^2 as a typical value, approximately 10 glands will be sampled by our device. This corresponds to a total sweat collection rate between 3 and 30 nL min^{-1}. This means, that between 90 and 900 nL is available for biosensing each 30 minutes, fulfilling the requirements for typical biosensors mentioned in the introduction. Furthermore, it is desired to sample sweat from single glands to be able to determine the number of active sweat glands and thereby determine the average sweat rate per gland.[23] Therefore, the chance that multiple sweat glands are located in the same collection chamber should be minimised. Using the probability model described in the ESI,† the probability of sampling 0, 1, or more than 1 gland per collection hole is calculated for our final design shown in Fig. 2. As expected, most collection holes will be empty, some will contain one sweat gland, and the chance that multiple sweat glands are present in a single collection hole is smaller than 0.5%. This discretised sampling strategy by using multiple collection holes thus allows for the sampling of sweat from single glands.

3.2 Creation and transport of droplets using electrowetting-on-dielectrics

Upon entry of sweat into the device through the collection holes, it needs to be transported towards the middle of the device, where the sensors are located. We have adopted electrowetting-on-dielectrics (EWOD) as the method to create droplets at the collection holes, and to subsequently transport them. EWOD is a technology that uses a voltage to modify the wetting properties of a liquid on a solid surface, allowing for the precise control of liquid movement. When the applied voltage is increased, the apparent contact angle

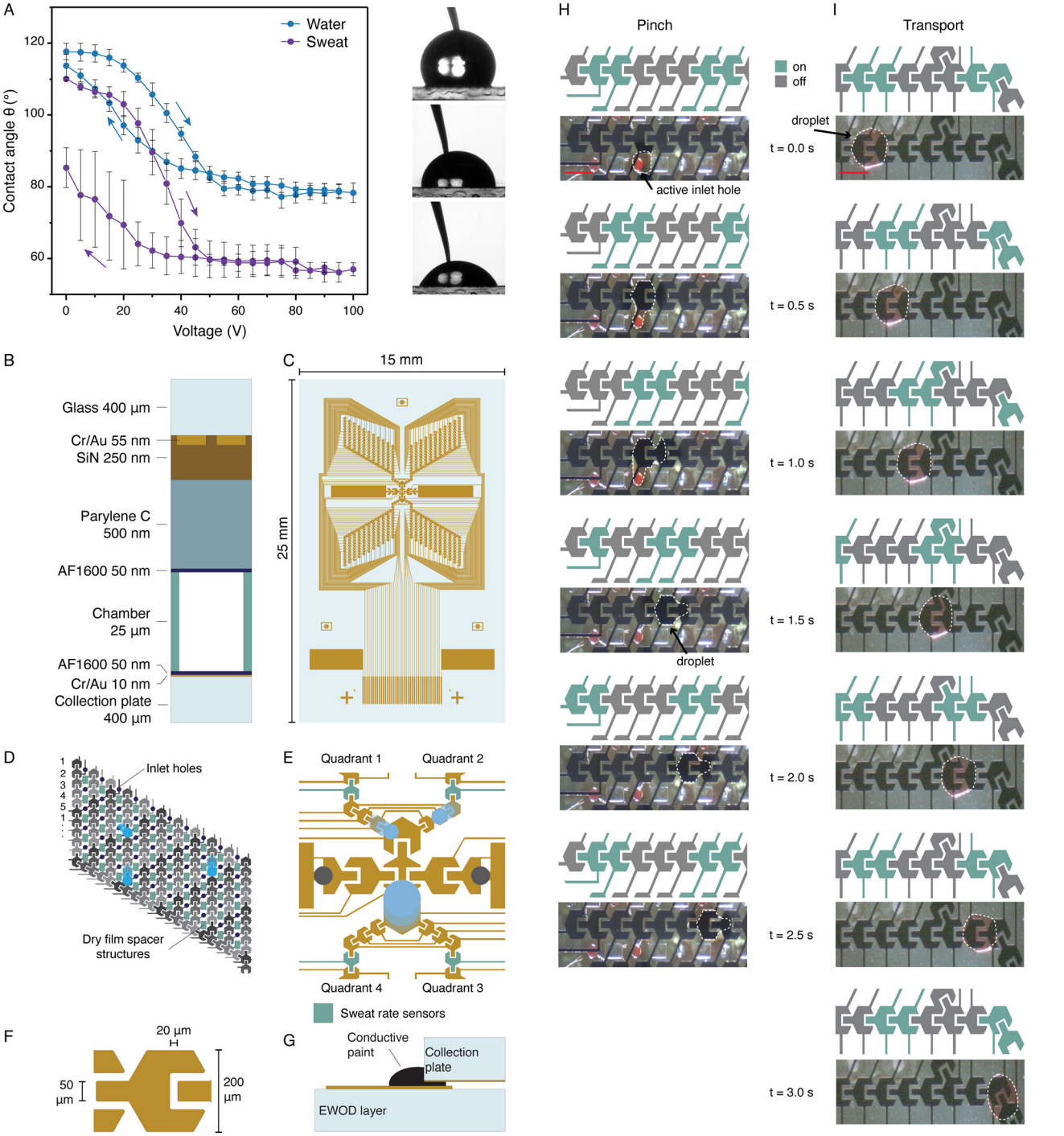

Fig. 3 Creation and transport of droplets using electrowetting-on-dielectrics (EWOD). (A) Contact angle of DI water and sweat from two healthy volunteers as a function of voltage. The maximum contact angle change is equal to 25–30° for both liquids. (B) Schematic representation of the EWOD stack. A double-layer dielectric stack is used to improve operational reliability. (C) Electrode pattern of the EWOD layer. Four identical quadrants transport droplets to the middle of the device. (D) The electrodes are grouped and activated in a wave with five steps for collection of droplets in the middle of the device. By connecting the electrodes in five groups, indicated by the labels 1 to 5, the number of electrical connections can be minimised. The inlet holes (purple circles) are located in between two columns of electrodes. In between the inlet holes, the dry film spacer structures (green rectangles) are located. (E) In the middle of the device, the electrodes are larger to facilitate the transport of larger or merged droplets towards the biosensor chamber or the waste absorber. The grey circles indicate the locations of the outlet holes towards the biosensor layer. Each quadrant has one electrode that is used as sweat rate sensor. (F) The electrodes have a hexagonal shape with a width of 200 µm. The hexagonal shape facilitates the connection of electrodes at a 30 degree angle. Each electrode has a protrusion overlapping the next electrode for successful transport. (G) Schematic illustration of the connection between the collection plate ground electrode and the connection pad electrode on the EWOD layer. A droplet of conductive paint is applied on the edge which makes an electrical connection. (H) Pinching of a nanolitre droplet of coloured DI water from an active inlet hole. The green electrodes are charged with 80 V_{AC} at a frequency of 1 kHz, with a switching time of 0.5 s. Scale bar equal to 200 µm. The dotted line indicates the droplet's edge. The full movie can be found in Movie S1.† (I) Transport of a coloured DI nanolitre water droplet by EWOD. The droplet follows the actuation wave towards the middle of the device. The green electrodes are charged with 80 V_{AC} at a frequency of 1 kHz, with a switching time of 0.5 s. Scale bar equal to 200 µm. The dotted line indicates the droplet's edge. The droplets can be transported with a switching time of 0.1 s (Movie S2†).

on the surface decreases, as displayed in Fig. 3A. The contact angle variation is studied for both water and sweat. The contact angle hysteresis of sweat is much larger than that of DI water, however, the maximum contact angle change, which is required for transport, remains 30 due to the lower saturated contact angle of sweat compared to water. This means that the electrowetting transport should in principle work equally wel for DI water and sweat. To maintain a time resolved measurement of sweat rate, the volume of the droplet should be small, in the nanolitre range. Consequently, the transfer velocity must be high enough to mitigate evaporation and to reduce the time to results. Another important aspect is the reliability of the transport, because the device needs to function continuously for hours, if not days. Conventionally, EWOD has been employed for typical actuated droplet volumes ranging from several microlitres to millilitres, with only a limited number of publications demonstrating manipulation down to the nanolitre scale.[24–26] Moving such small droplets is mostly done in an oil environment rather than in air, due to the lower surface tension and the smaller effect of evaporation. We are the first to show reliable transport of droplet volumes down to 50 pL in air using EWOD (see the ESI† and Fig. S3). To ensure reliable EWOD operation, we employ a multilayered dielectric stack consisting of an inorganic silicon nitride layer and an organic parylene C layer which prevents dielectric breakdown, complemented by a PTFE AF1600 coating to maintain a high initial contact angle (θ_0) (Fig. 3B). Additionally, the surface is impregnated with 20 cSt silicone oil, which we found to enhance pinching, transport, and overall reliability within the time frame of our experiments. The oil forms a thin layer on top of the hydrophobic coating, without having to fill the whole EWOD chamber which would lead to leakage of oil out of the device. To enable the transport of sweat from all 200 collection holes to the sensor locations, a butterfly-like design is developed (Fig. 3C). Each quadrant has 50 collection holes (Fig. 3D), which are connected by columns of electrodes, guiding sweat droplets to the middle of the device (Fig. 3E). The dimensions and design of the EWOD electrodes, shown in Fig. 3F, are crucial for pinching and transport of small droplets. The electrode width measures 200 μm and the chamber height (h_c) is 25 μm. Protrusions on the electrodes facilitate the transport of droplets to the adjacent electrode, optimising the transport. At the centre, all four quadrants converge to larger electrodes, which serve as a buffer to decrease the likelihood of flooding as the larger electrodes are able to transport larger droplets which could for instance be created by the merging of droplets arriving from different quadrants. Furthermore, a bifurcation and two outlet holes are located in the middle of the device, as shown in Fig. 3E. This bifurcation design is implemented for the integration of a biosensor, as explained in section 3.4. Rectangular dry film structures are fabricated on top of the collection plate, indicated in green in Fig. 3D. These structures ensure that the EWOD chamber height of 25 μm is maintained over the whole area of the device. The collection plate is covered with a thin layer of chromium/gold (Cr/Au) to realise the ground electrode for EWOD actuation. The collection plate, including the dry film structures, is also covered with a layer of AF1600 hydrophobic coating for successful EWOD transport. After attaching the EWOD layer to the collection plate with double sided tape, two droplets of conductive paint are applied to the two outer collection pads on the EWOD layer, to attach the collection plate electrode (Fig. 3G). A common challenge in devices employing multiple electrodes is the management of numerous electrical connections. Our design circumvents this issue by the fact that all electrodes are organised in sets. Each set contains five electrodes labelled 1–5 (Fig. 3D). All electrodes of all sets having the same number are electrically connected to each other; hence per quadrant, containing 125 electrodes, there are only 5 connections to the actuation set-up required. Furthermore, an electric circuit is designed that connects all electrodes with the same number in a quadrant while not crossing the electrical circuits of the electrodes with other numbers, hence no through glass vias are required in the electrical circuit design (Fig. 3C). However, by connecting all electrodes of one step in series, the risk of dysfunctional electrodes due to a small break in the line is increased. Therefore, all four quadrants of the device are connected separately, which minimises the risk of total device failure in the event of a minor defect in one of the interconnects, as this only disrupts the operation of one quadrant. Additionally, the independent quadrant configuration offers greater flexibility, enabling the activation of more or less EWOD electrodes depending on the availability of sweat. We used the previously developed artificial skin platform[18] to evaluate the pinching of droplets and the transport using EWOD. In these experiments, DI water was used as a proxy for sweat (±99% water), and the water was coloured using food dye for increased visibility. Fig. 3H and Movie S1† demonstrate the pinching of a nanolitre droplet from a protrusion emerging from a collection hole in the integrated device, which is placed on the artificial skin. When the electrical wave passes by, the protrusion has enough overlap with the EWOD electrodes and a droplet gets pinched and is then transported to the right. Fig. 3I shows a time lapse of the successful transport of a nanolitre droplet in the integrated device. The transport of a droplet can be as fast as 0.1 seconds per time step (Movie S2†).

3.3 Design and characterisation of sweat rate measurement

As several biomarkers in sweat are sweat rate dependent,[27] it is important that a sweat sensing platform has the capability to measure the sweat rate. Thermal flow meters are the most commonly used sensors to measure microfluidic flows.[28] However, this is not a solution at the low flow rates we are dealing with in our sweat sensing application. Therefore, we have implemented a capacitive measurement that exploits the electrowetting electrodes (Fig. 4A) and counts the passing

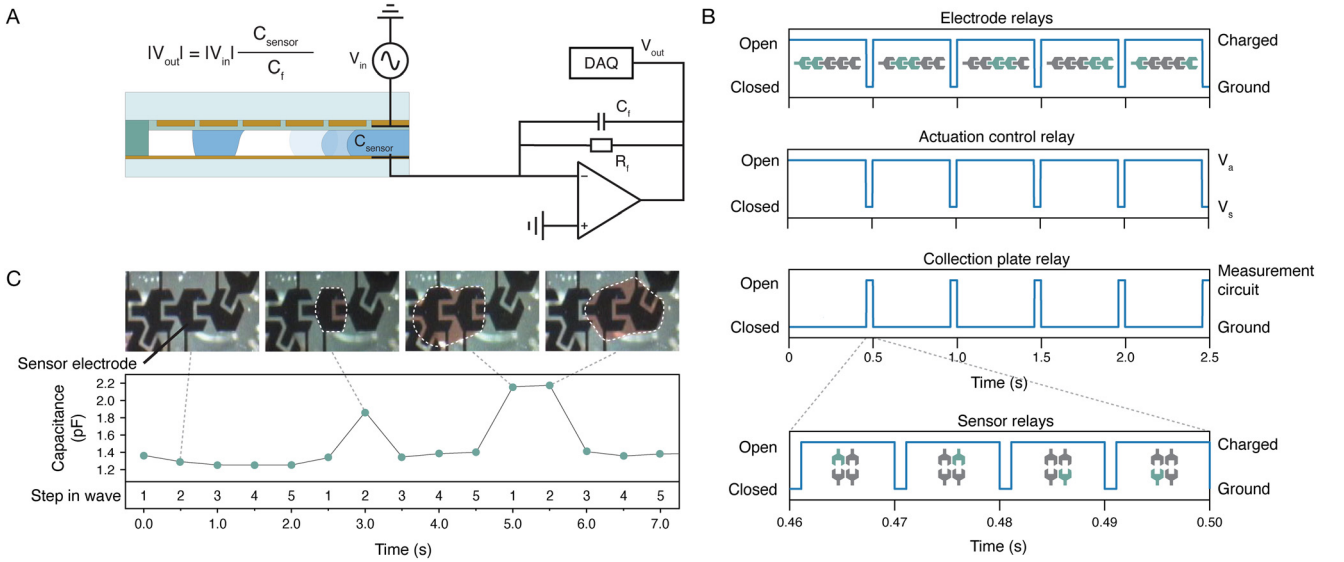

Fig. 4 Design and characterisation of sweat rate measurement. (A) Schematic of the capacitance measurement of a droplet. The difference in the capacitance of sweat/water compared to air enables the detection of a droplet. To measure the capacitance, a measurement voltage (V_{in}) of 5 V_{AC} is applied to the sensor electrode. (B) Schematic of the timing of the relays. The control PCB contains 37 electrode relays, one actuation control relay and one collection plate relay. The four sensors are controlled with the electrode relays. The electrode relays switch the electrodes between ground and signal. The actuation control relay controls which channel of the waveform generator is connected to signal. The collection plate relay switches the collection plate electrode between ground (for EWOD actuation) and the measurement circuit (during sensing). (C) Capacitive sensing for droplet detection. The graph displays the measured capacitance after each actuation step in the wave. The difference between a single and a double droplet can be seen in the measured capacitance, because the latter is present for two steps in the wave instead of one.

droplets. Each quadrant has one sweat rate sensor, which is an electrode that is decoupled from the electrodes connected in the wave (Fig. 3E). The difference in capacitance between air and liquid allows for the detection of a droplet passing over the sensor electrode. A measurement voltage (V_{in}) must be applied to the sensing electrode to measure the capacitance, and the magnitude of this voltage should be small enough to ensure that the measurement signal does not move the droplets. However, the capacitance (C_{sensor}) is expected to be low due to the presence of the dielectric layers, namely in the range of 1–5 pF, and therefore a small V_{in} will only generate a small current. One can consider to direct the small current through a large resistor, to enhance the voltage. However, electrical fields in the environment will create voltages over the resistor as well, inducing noise currents which can reduce the sensor sensitivity. Therefore, the small current is directly fed into an operational amplifier rather than through a resistor. Because the amplifier enhances the difference between the inverting input and the non-inverting input, noise signals originating from the environment both present at the inverting and the non-inverting input are reduced. By switching the collection plate electrode from the ground to the measurement circuit and by charging the EWOD electrodes which function as sensor with the measurement signal, a measurement can be recorded (Fig. 4B). Data is recorded within a period of 10 ms using a data acquisition unit (DAQ) and a fast Fourier transform (FFT) is performed to obtain the amplitude at the measurement frequency of 5 kHz. The conversion using FFT acts as a digital filter by eliminating the disturbances in the other frequencies. Detailed information on the capacitive sensing method is provided in the ESI.† The capacitive sensing principle is used to detect passing droplets. After each actuation step, the capacitance of the sweat rate sensors is measured. Each sweat rate sensor electrode is integrated in one of the actuation electrode sets; in each set, the electrodes are numbered from 1 to 5 and electrode 2 has the dual function of actuation and sensing. This means that the expected increase in capacitance is detected after the second step in the wave. Fig. 4C shows the capacitance measured by the sweat rate sensor. The first wave, *i.e.* the first 2.5 seconds of the signal, does not contain a droplet and therefore no peak is detected. The second wave shows a distinct peak in the measurement after the second step, indicating the presence of a droplet. The third wave shows an increased capacitance after both the first and second step, caused by a larger droplet passing the sensor. Such a large droplet can be caused by the merging of droplets from two different branches, or the pinching of a larger droplet from the collection hole. By assuming an average size of the droplets, the total sweat volume passing the sensor per time can be calculated by multiplying droplet volume by the number of passing droplets that are detected. Since we know the total surface area the droplets originate from (because we have one capacitive sensor per quadrant, as shown in 3C and E, and we know the sampled area, since it is determined by the total area of all collection chambers in one quadrant), we can calculate the sweat rate in terms of volume per time per

surface area. The range of sweat rates we can measure is very large, since the measurement time of the capacitance change is very fast (namely 10 ms), hence the limit is determined be the rate at which droplets move over the sensing electrode.

3.4 Biochemical sensor integration

The main aim of our paper is to provide proof-of-principle of the fluidic principle of our sweat sensing device, and we can measure sweat rate as shown in the previous section, but the currently presented integrated devices do not contain a biosensor yet. However, a biosensor layer is designed which enables the integration of a biosensor (Fig. 5). The biosensor layer is located on the EWOD glass substrate, on the side opposite to the EWOD electrodes, and therefore no EWOD actuation takes place in this layer. The biosensor layer consists of two regions as indicated in Fig. 5A. In one region, a porous paper waste absorber can be placed for removal and evaporation of sweat. The other region contains a chamber engraved in the glass in which a biosensor can be placed (Fig. 5C). The current biosensor chamber has a height of 40 μm, a width of 460 μm, and a length of 5 mm, resulting in a volume of 92 nL. The time resolution of the biosensor measurements is related to the number of sampled glands and the sweat rate per gland. Assuming a sweat collection rate between 3 and 30 nL min^{-1}, as above, this biosensor chamber will fill in approximately 30 to 3 minutes. Both regions of the biosensor layer are separately accessed through two outlet holes from the EWOD layer. These through-glass holes have a diameter of 200 μm on the EWOD layer side and a diameter of 460 μm on the biosensor layer side. A glass plug is designed and fabricated, which is placed into this hole, forming a very thin (<5 μm) channel between the wall of the outlet and the plug. Since the glass plug is hydrophilic, it aids the transport of sweat through the outlet. Furthermore, the plug decreases the volume of the hole significantly. A bifurcation electrode is integrated in the middle of the EWOD electrode design, as shown in Fig. 3E. Using this bifurcation electrode, sweat can be directed either towards the outlet hole at the waste absorber, or towards the outlet hole at the biosensor chamber. This split towards two regions is created to facilitate the use of biosensors that need stabilisation or hydration time, like most electrochemical biosensors with enzymes. When the biosensor chamber is filled (Fig. 5D), sweat can be temporarily directed towards the waste absorber. Once the biosensor has hydrated or stabilised, new droplets of sweat can be directed towards the biosensor chamber. A diverging chamber is located at the end of the biosensor chamber. When fresh droplets of sweat are directed towards the biosensor chamber, this diverging chamber fills and directs the sweat towards the waste absorber. The absorbing capillary strength of the waste

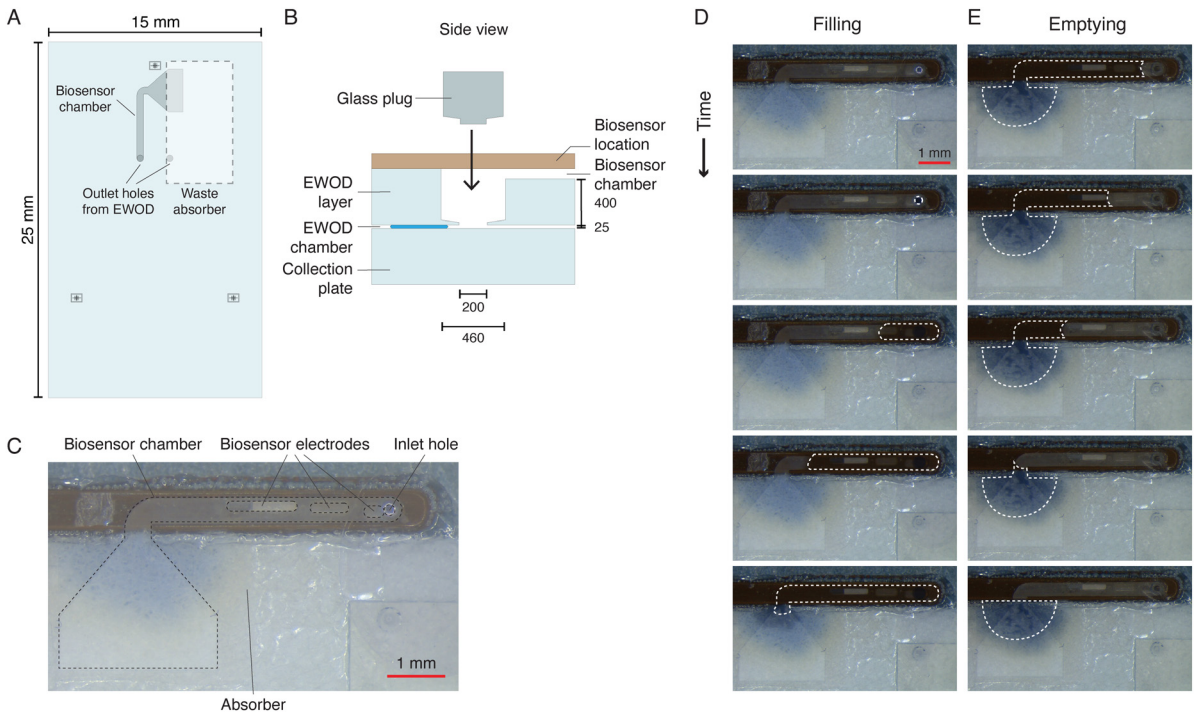

Fig. 5 Design of the biosensor layer. (A) Schematic of the biosensor layer containing the two outlet holes from the EWOD layer, a biosensor chamber on top of which the biosensor can be placed, and a waste absorber. (B) Side view of the outlet hole from the EWOD layer to the biosensor layer. The brown rectangle indicates the location for a biosensor. A hydrophilic glass plug is placed in the outlet hole during assembly of the device to aid transport of sweat from the EWOD chamber to the biosensor layer and to reduce the required volume. Dimensions are indicated in μm unless noted otherwise. (C) Photograph of a commercial glucose biosensor attached on top of the biosensor chamber. (D and E) Time-lapse of the filling (D) and emptying (E) of the biosensor chamber. The full movie can be found in Movie S3.†

absorber is large enough to completely empty the biosensor chamber and thus remove all sweat from the biosensor chamber (Fig. 5E). When, after emptying, the biosensor chamber again fills, a new measurement can be executed, after which sweat is again absorbed in the waste absorber and the cycle is repeated. Depending on the sweat collection rate, the repeat time, and thus the measurement rate, is typically 3 to 30 minutes, *i.e.*, the filling time of the biosensor chamber, for measurements on the fingertip, consistent with the requirement of 5 to 30 minutes mentioned in the introduction.

3.5 Device evaluation on artificial skin

We used our earlier developed artificial skin platform[18] to evaluate the working principle of the integrated device (Fig. 6A). Fig. 6B and C display the sweat sensor signal output of one of the four sensors of an integrated device placed on the artificial skin, operated at high and low flow rates, respectively, and carried out with different devices. After each EWOD actuation step, a measurement is executed for 10 ms (see Fig. 4B); each dot in the upper panels of Fig. 6B and C represents a measurement. A wave has five steps, and thus five measurements are done in one cycle. A droplet is detected if the difference between the value of the measurement of step 2 and step 4 in the wave is more than 3.5 times the standard deviation of the total signal; these instances are indicated in the middle panels. If the difference between step 2 and step 1 is less than the standard deviation, a double droplet is registered, indicated with a darker blue bar. The flow rate in nL min^{-1}, shown in the lower panels, is calculated by multiplying the droplet count with the average droplet size of 1.06 nL. This droplet size was determined experimentally by analysing the droplet area using image analysis (ImageJ) and assuming a height of 25 μm. The flow rates displayed in Fig. 6B and C are running averages using window sizes of 1 minute and 10 minutes, respectively. Clearly, the trend of the measured flow rate corresponds to that of the set flow rate of the artificial skin. For the high flow rate setting, a sweat rate between approximately 5 and 15 nL min^{-1} was measured; for the low flow rate setting, a value of around 1 nL min^{-1} was obtained. From these values, the measured sweat rate per surface area can be calculated by dividing by the collection area of one quadrant, being 0.048 cm^2 (see the ESI†), since these are measurements from one sensor, which results in 104–313 and 21 nL min^{-1} cm^{-2}, for the high and low flow rate settings respectively. The flow rate through the artificial skin was not measured and therefore no quantitative comparison can be made between the applied and the measured flow rates. Important to note, is that Fig. 6C proves the longer-term operation of our device. For a period of 55 minutes, the device is activated, and droplets are collected, pinched, transported and sensed. The baseline of the sweat rate sensor signal is stable during actuation, and we confirmed by visual inspection

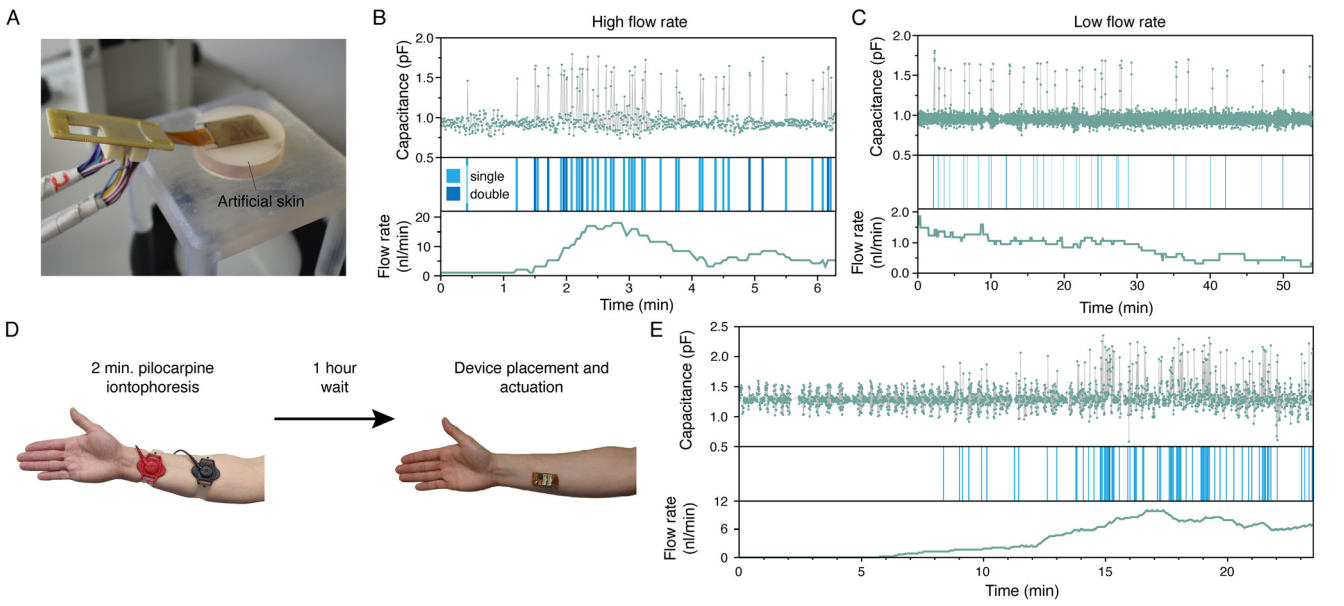

Fig. 6 Integrated device evaluation. (A) Device on artificial skin. (B and C) Sweat rate measurement on the artificial skin at high (B), and low (C) flow rate. Note the difference in the scale of the *x*-axis. The peaks in the capacitance measurement are recorded and represent the passage of a single (light blue) or double (dark blue) droplet. An indication of the sweat rate is obtained by multiplication of the number of detected droplets with the average droplet size and calculating a running average. The window of the running average has a width of 1 or 10 minutes for the high and low flow rate, respectively. (D) Device on skin. A short 2 min pilocarpine iontophoresis is performed on the forearm. The device is placed on the stimulated area 1 hour after stimulation. (E) Sweat sensor signal of the device on human skin. The peaks correspond to droplets of sweat passing over the sweat rate sensor an indication of the sweat rate is obtained by multiplication of the number of detected droplets with the average droplet size and calculating a running average. The window of the running average has a width of 5 minutes.

through a microscope that all droplets are recorded by the sweat rate sensor.

The analysis of the measured signals can be improved and extended further. First, the variation in the measured capacitance output suggests that there is a variation in the droplet size. A preliminary analysis (see ESI†), shows that the linearity between the sensor capacitance and the area of the sensor electrode that is covered by a droplet can give an estimation of the actual droplet size. Using this approach can result in a more accurate flow rate estimation than using an average droplet size. Second, by a more in-depth analysis of the pattern of passing droplets, more information may be extracted. Natural sweat secretion has a pulsatile nature,[29] which means that the sweat production per gland shows a distinct pattern in time with sweat bursts and inactive periods. By analysing the pattern of passing droplets, it is in principle possible to extract how many sweat glands are sampled, without prior knowledge about the number of active sweat glands.[23] From this information, the sweat rate per gland can be calculated which is a unique attribute for a sweat sensing device.

3.6 On-body device evaluation

After successful testing on the artificial skin, we carried out tests on healthy volunteers to obtain proof-of-concept of the wearable sweat sensing device on-body. Prior to the experiments, the used devices were optically and electrically characterised. Quadrants with defects or shortcuts were turned off in the control software. Before applying the device, the skin was cleaned with water, soap and acetone. Furthermore, a thin layer of petroleum jelly was applied to the skin for increasing the contact angle of the skin and reducing leakage of sweat through the skin topography, as mentioned before. The first experiments were executed with the device placed on the fingertip of two volunteers in resting state. Unfortunately, no entry of sweat was detected during 2.5 hour operation of the device. We believe there can be two reasons for this observation: (1) there was leakage of sweat between the medical tape and the skin or (2) the required inlet pressure of the device was higher than the pressure delivered by the sweat glands. Since the volume produced by sweat glands in resting state is low, and if sweat would be leaking or if the topography of the skin would create a larger reservoir than we anticipated, there is not enough sweat available for entry into the device. Furthermore, once sweat starts leaking, it is possible that the available pressure is not sufficient anymore to overcome the Laplace pressure for entry into the device. It is also possible that we have overestimated the pressure delivered by the sweat glands at low flow rates. If the required inlet pressure, which is around 2.6 kPa in the current design, cannot be delivered by the sweat glands, sweat will not enter the device. To verify the working principle of the devices, we conducted a brief 2 minute iontophoretic sweat stimulation prior to the experiment using the Macroduct stimulation device, to artificially increase the pressure exerted by the sweat glands.[22] This procedure could reveal whether an excessive required inlet pressure is the factor impeding the entry of sweat into the devices. The stimulation cannot be done on the finger, due to the dimensions of the electrodes of the Macroduct device, and therefore we applied it on the forearm. The pilocarpine iontophoretic stimulation is known for its initial high burst in sweat production, which could lead to flooding of our device because it is designed to operate at low sweat rate conditions. To circumvent this initial sweat burst and to avoid flooding of the device, the device was applied to the skin one hour after stimulation and the experiment was started (Fig. 6D). Fig. 6E shows the resulting sweat rate sensor signal of one quadrant of the device. After an initial filling time of the collection holes of about 8 minutes, sweat entered the device and droplets were detected by the sweat rate sensor. Using the analysis described above, an average flow rate of 3.9 nL min^{-1} is obtained. Taking into account the sampling area of one quadrant (0.048 cm^2, see the ESI†), this corresponds to a sweat rate per area of 81 nL min^{-1} cm^{-2}, which is in the low range of sweat rate we expect for an individual in resting state. This experiment demonstrates the working principle of the device based on discretised microfluidics, on-skin, and with real sweat. Our current integrated devices can capture and transport sweat droplets and measure approximate sweat rate. Movies recorded during the on-body experiments can be found in the ESI† (Movies S4 and S5).

4 Conclusions

We have presented a wearable integrated device and method enabling on-skin sweat sensing of human individuals in resting state by utilising discretised microfluidics to actively handle minute amounts of sweat. The device can collect sweat produced by sweat glands, it can pinch, and transport nanolitre sweat droplets using electrowetting-on-dielectrics (EWOD), and it can detect passing droplets using capacitive sensors which provides a measurement of the sweat rate. By evaluation on our artificial skin platform operated at low and high flow rates, we verified that the devices can operate at the low flow rate corresponding to the sweat rate of individuals in rest. We measured sweat rates from 21 to 313 nL min^{-1} cm^{-2}, fitting with the expected range on the fingertips of individuals at rest, which is 15 to 150 nL min^{-1} cm^{-2}. By having a multitude of collection holes with a small volume, we enable the collection of sweat within a clinically relevant time frame of up to approximately 30 minutes. After collection, the sweat can be transported towards the sensors as small droplets in seconds. We integrated a biosensor chamber with a volume of approximately 100 nL, which fills within up to 30 minutes, simultaneously with the collection. Hence, the maximum delay time between the sample taking from the skin, as well as the maximum time between measured data points, is 30 minutes for the very lowest sweat rates expected, which

fulfils the requirements stated in the introduction. In tests on individuals in resting state, however, no sweat entered the devices unless pilocarpine iontophoretic stimulation was briefly applied one hour before applying the device and starting the measurement. Then, the sweat collection and transport did work at a measured sweat rate of 81 nL min^{-1} cm^{-2}, again within the range for individuals at rest. Elimination of the stimulation, which is desired for health monitoring in the clinic, requires a redesign of the skin-device interface. We hypothesise that the main cause for the sweat not entering the device in the tests with individuals in resting state, is that the sweat glands cannot deliver the required inlet pressure and thus the inlet pressure of the device needs to be lowered. This can be achieved with geometrical changes or adaptation of the wetting properties of the used materials. The trend of the measured sweat rate correlates with that of the sweat rate generated by the artificial skin, but the quantitative relationship between the droplet detection and the generated sweat rate per surface area is to be verified. We provide proof-of-principle of the fluidic principle of our sweat sensing device as well as the sweat rate measurement, but we do not show biosensing. We designed and fabricated a biosensor layer in which a biosensor can be integrated provided it fits in the available volume of the biosensor chamber. Biosensing experiments are subject of our ongoing research, and this work will be published in the future. We aim for measuring biomarkers such as glucose, cortisol, lactate, and urea. The incorporation of different biomarker sensors in the device opens a wide field of applications with a large potential impact on health monitoring. We designed the device for operation on the fingertip, but it can be tailored to be used on different body locations, with different sweat gland densities and sweat rates per gland. For instance, on a body location with a lower sweat gland density, the collection area of the device can be increased in order to sample enough sweat glands, and in locations with a higher average sweat rate per gland, the EWOD electrodes can be increased to transport larger droplets or the EWOD velocity can be increased to transport more droplets in the same period to avoid flooding. More characterisation is required in the future to establish the suitability of our device for the wide range of sweat properties of different individuals. Eventually, a clinical trial with patients will be performed to validate the use of sweat for gathering clinical information. For the implementation of the device into the clinical workflow, recent clinical case studies on the clinical relevance of sweat sensing[30] can be extended to the device functionality in clinical practice, and the fitting in the workflow. This paper presents the first demonstration of EWOD controlled liquid manipulation integrated in a wearable device. The sweat collection, transport and sweat sensing utilising nanolitre sized sweat droplets is a unique application of EWOD, which enables to expand lab-on-chip functionality in wearable devices.

Data availability

All the anonymised raw and analysed datasets generated during the study are available from the authors on request.

Author contributions

Conceptualization: EJMM, EP, JMJDT methodology: EJMM, EP investigation: EJMM, WV visualization: EJMM supervision: EP, JH, JMJDT writing – original draft: EJMM writing – review and editing: EJMM, EP, JH, JMJDT funding acquisition: EP, JMJDT.

Conflicts of interest

There are no conflicts to declare.

Acknowledgements

This project was supported by the penta programme (project 19017).

References

1 E. J. Moonen, J. R. Haakma, E. Peri, E. Pelssers, M. Mischi and J. M. J. den Toonder, *View*, 2020, **1**, 20200077.
2 Y. Wu, X. Li, K. E. Madsen, H. Zhang, S. Cho, R. Song, R. F. Nuxoll, Y. Xiong, J. Liu, J. Feng, T. Yang, K. Zhang, A. J. Aranyosi, D. E. Wright, R. Ghaffari, Y. Huang, R. G. Nuzzo and J. A. Rogers, *Lab Chip*, 2024, **24**, 4288–4295.
3 Y. Zhang, Y. Chen, J. Huang, Y. Liu, J. Peng, S. Chen, K. Song, X. Ouyang, H. Cheng and X. Wang, *Lab Chip*, 2020, **20**, 2635–2645.
4 M. J. Buono and K. P. Connolly, *J. Therm. Biol.*, 1992, **17**, 267–270.
5 N. A. Taylor and C. A. Machado-Moreira, *Extrem. Physiol. Med.*, 2013, **2**, 4.
6 G. E. Burch and W. A. Sodeman, *Am. J. Physiol.*, 1943, **138**, 603–609.
7 Q. Cao, B. Liang, T. Tu, J. Wei, L. Fang and X. Ye, *RSC Adv.*, 2019, **9**, 5674–5681.
8 Y. Yang, S. Xing, Z. Fang, R. Li, H. Koo and T. Pan, *Lab Chip*, 2017, **17**, 926–935.
9 E. Garcia-Cordero, F. Bellando, J. Zhang, F. Wildhaber, J. Longo, H. Guérin and A. M. Ionescu, *ACS Nano*, 2018, **12**, 12646–12656.
10 H. Y. Y. Nyein, M. Bariya, B. Tran, C. H. Ahn, B. J. Brown, W. Ji, N. Davis and A. Javey, *Nat. Commun.*, 2021, **12**, 1823.
11 N. B. Twine, R. M. Norton, M. C. Brothers, A. Hauke, E. F. Gomez and J. Heikenfeld, *Lab Chip*, 2018, **18**, 2816–2825.
12 X. Hong, H. Wu, C. Wang, X. Zhang, C. Wei, Z. Xu, D. Chen and X. Huang, *ACS Appl. Mater. Interfaces*, 2022, **14**, 9644–9654.
13 R. Peng, Z. Sonner, A. Hauke, E. Wilder, J. Kasting, T. Gaillard, D. Swaille, F. Sherman, X. Mao, J. Hagen, R. Murdock and J. Heikenfeld, *Lab Chip*, 2016, **16**, 4415–4423.

14 J. Min, S. Demchyshyn, J. R. Sempionatto, Y. Song, B. Hailegnaw, C. Xu, Y. Yang, S. Solomon, C. Putz, L. E. Lehner, J. F. Schwarz, C. Schwarzinger, M. C. Scharber, E. Shirzaei Sani, M. Kaltenbrunner and W. Gao, *Nat. Electron.*, 2023, **6**, 630–641.
15 P. Simmers, S. K. Li, G. Kasting and J. Heikenfeld, *J. Dermatol. Sci.*, 2018, **89**, 40–51.
16 A. Schultz, S. Chevalliot, S. Kuiper and J. Heikenfeld, *Thin Solid Films*, 2013, **534**, 348–355.
17 V. Srinivasan, V. K. Pamula and R. B. Fair, *Lab Chip*, 2004, **4**, 310.
18 E. J. M. Moonen, T. Ul Islam, S. van Kemenade, E. Pelssers, J. Heikenfeld and J. M. J. den Toonder, *Lab Chip*, 2023, **23**, 2268–2275.
19 Z. Sonner, E. Wilder, J. Heikenfeld, G. Kasting, F. Beyette, D. Swaile, F. Sherman, J. Joyce, J. Hagen, N. Kelley-Loughnane and R. Naik, *Biomicrofluidics*, 2015, **9**, 031301.
20 K. Sato, A. Nishiyama and M. Kobayashi, *Am. J. Physiol.*, 1979, **237**, C177–C184.
21 I. J. Schulz, *J. Clin. Invest.*, 1969, **48**, 1470–1477.
22 J. Choi, Y. Xue, W. Xia, T. R. Ray, J. T. Reeder, A. J. Bandodkar, D. Kang, S. Xu, Y. Huang and J. A. Rogers, *Lab Chip*, 2017, **17**, 2572–2580.
23 J. Haakma, E. Peri, S. Turco, E. Pelssers, J. M. J. Den Toonder and M. Mischi, *2022 IEEE 21st Mediterranean Electrotechnical Conference MELECON*, Palermo, Italy, 2022.
24 Y.-Y. Lin, R. D. Evans, E. Welch, B.-N. Hsu, A. C. Madison and R. B. Fair, *Sens. Actuators, B*, 2010, **150**, 465–470.
25 W. C. Nelson and C.-J. Kim, *J. Microelectromech. Syst.*, 2011, **20**, 1419–1427.
26 Y.-Y. Lin, E. R. Welch and R. B. Fair, *Sens. Actuators, B*, 2012, **173**, 338–345.
27 L. B. Baker, *Temperature*, 2019, **6**, 211–259.
28 C. Cavaniol, W. Cesar, S. Descroix and J.-L. Viovy, *Lab Chip*, 2022, **22**, 3603–3617.
29 T. Nishiyama, J. Sugenoya, T. Matsumoto, S. Iwase and T. Mano, *Auton. Neurosci.*, 2001, **88**, 117–126.
30 S. Adelaars, C. J. Konings, L. Cox, E. Boonen, M. Mischi, R. A. Bouwman and D. Van De Kerkhof, *Clin. Chem. Lab. Med.*, 2024, **62**, 1118–1125.